Collective dynamics of domain walls: An antiferromagnetic spin texture in an optical cavity

Jephthah O. Iyaro [1,*], Igor Proskurin [1,2,†] and Robert L. Stamps[1,‡]

[1]*Department of Physics and Astronomy, University of Manitoba, Winnipeg, Manitoba, Canada R3T 2N2*

[2]*Institute of Natural Sciences and Mathematics, Ural Federal University, Ekaterinburg 620002, Russia*

(Received 4 March 2021; revised 9 October 2021; accepted 2 November 2021; published 15 November 2021)

Spin canting and complex spin textures in antiferromagnetic materials can be described in terms of Dzyaloshinskii-Moriya interactions (DMI). Values for DMI parameters are not easily measurable directly, and often inferred from other quantities. In this work, we examine how domain wall dynamics in an antiferromagnetic optomagnonic system can display unique features directly related to the existence of DMI. Our results indicate that the presence of DMI enables spin interactions with cavity photons in a geometry which otherwise allows no magneto-optical coupling, and on the other hand modulates frequencies in a geometry where coupling is already realized in the absence of DMI. This result may be used to measure the DMI constant in optomagnonic experiments by comparing resonances obtained with different polarizations of the exciting field.

DOI: 10.1103/PhysRevB.104.184416

I. INTRODUCTION

Cavity optomagnonics in which precision measurements of interactions between photons and magnons are studied [1] has potential applications in quantum information processing [2] and spintronics [3]. Essentially, it allows a description where the force on magnetic moments appears as an optical pressure of photons. We discuss here an optomagnonic analog of cavity optomechanics [4] in which one is able to observe the coupling of electromagnetic radiation to spin texture oscillations [1,5]. As a consequence, one is able to realize optomechanical phenomena in magnonic systems, which includes mode attraction—the coalescence of two eigenmodes marked by two exceptional points [6]. Described as an anticrossing gap in Ref. [7] where the coupling between a microwave cavity mode and a ferromagnetic magnon mode was studied, this behavior has continued to gain attention and has been observed experimentally in the microwave regime in a planar geometry [8] and in a microwave cavity [9] with frequencies in GHz range. The physical mechanisms behind level attraction in these cavity-magnonic experiments have been proposed as dissipative coupling [10–12] and also attributed to an instability in optomechanical systems associated with a negative frequency in the effective Hamiltonian of an externally driven system [13,14].

Cavity magnonics has been explored primarily for ferromagnetic systems, with frequencies in the GHz range [15–21]. At present, antiferromagnets are receiving attention as possible platforms for exotic spin textures such as skyrmions, which can exist in low-dimensional materials with broken inversion symmetry. Antiferromagnets are characterized by dynamics in the THz range [22], typically have large magnetic anisotropies and zero net magnetization that make them useful for spintronic applications, but at the same time makes experimental observation of collective magnetic dynamics difficult. Here, we propose to use magneto-optical coupling, which is a well established experimental technique to study ultrafast dynamics in antiferromagnetic insulators [23] to study the collective motion of antiferromagnetic textures.

The Dzyaloshinskii-Moriya interaction (DMI) can exist in noncentrosymmetric magnetic materials and is known to play an important role in describing nontrivial spin textures [24,25]. In one spatial dimension, DMI can lead to long-periodic modulated structures known as soliton lattices, while in two spatial dimensions DMI helps to stabilize topologically nontrivial skyrmion lattices. It is also known to play an important role in domain walls [26,27], where it affects the domain wall structure and lifts degeneracy between domain walls with opposite chiralities. In this paper, we show that DMI can also affect how spin textures are coupled to optical photons.

Optomagnonics opens the possibility of coupling electromagnetic waves to nonuniform magnetic ground states such as a magnetic vortex in a microdisk [28]. Whereas some of the most interesting textures are found in two and three dimensions, there have been some studies on one-dimensional structures such as solitons in antiferromagnets [29–31] and helimagnets [32,33]. Here, we examine the case of the coupling of optical cavity photons to a domain wall. Domain walls are one-dimensional topological textures whose dynamics can be described in analogy to that of massive particles [34,35]. The collective motion of ferromagnetic and antiferromagnetic domains walls is well studied [35–41].

Coupling of collective magnon modes to optical cavity modes have been realized in a number of experiments [20,42]. Recently, a model for cavity magnonics with a ferromagnetic domain wall was proposed and parameters for the coupling were estimated [43]. In that case the frequency of the ferromagnetic domain wall oscillation in a pinning site is in the GHz range.

*iyaroo@myumanitoba.ca

†Igor.Proskurin@umanitoba.ca

‡Robert.Stamps@umanitoba.ca

In this paper, we discuss a cavity optomagnonic system where an antiferromagnetic domain wall is coupled to optical photons via the inverse Faraday effect [23,44,45]. This leads to a nonlinear optomechanical-type coupling where the domain wall reacts to pressure from cavity photons. We discuss the hybridization of optical and magnonic modes and identify a level attraction regime.

We also investigate the effects of DMI on the domain wall dynamics in two different geometries. We find that, in one geometry, where DMI favors one chirality of the domain wall, the presence of DMI enables coupling of magnons to photons which is otherwise nonexistent without DMI. In a second geometry, the DMI exerts a torque which leads to the domain wall tilt and consequent effects on the coupling terms. We expect that these features are not limited to the case of a single domain wall and can be found in other chiral spin textures. This can assist detection and quantification of DMI in thin films of antiferromagnetic materials.

II. MODEL

Our model assumes a Néel domain wall in a one-dimensional antiferromagnet as shown in Fig. 1(a). Sublattices A and B have opposite spins, S_A and S_B, respectively. The preferred magnetization rotation plane is the x-z plane. The Hamiltonian describing this system is

$$\mathcal{H}_{\rm dw} = \sum_{\langle i,j\rangle} J\vec{S}_i\cdot\vec{S}_j - K_z\sum_i(\vec{S}_{i,z})^2 - \sum_i K_x(\vec{S}_{i,x})^2 + \sum_i(-1)^{i+1}\vec{D}\cdot(\vec{S}_i\times\vec{S}_{i+1}). \quad (1)$$

The first term on the right is the nearest-neighbor exchange interaction between spins on the sublattices. The second and third terms are the uniaxial anisotropies in the z and x directions, respectively [46], with constants $K_z \gg K_x$. The last term is the antisymmetric interfacial DMI whose alternating sign prevents a spiral spin state [47].

We introduce the total and staggered magnetizations, $\vec{m}_i = (\vec{S}^i_A + \vec{S}^i_B)/2S$ and $\vec{l}_i = (\vec{S}^i_A - \vec{S}^i_B)/2S$, respectively, subject to the constraints that $\vec{m}\cdot\vec{l} = 0$ and $\vec{m}^2 + \vec{l}^2 = 1$ [35,38,48,49]. Going by this definition, we make the substitutions, $\vec{S}^i_A = S(\vec{m}_i + \vec{l}_i)$ and $\vec{S}^i_B = S(\vec{m}_i - \vec{l}_i)$, into Eq. (1). This results in a sum over lattice points rather than spins. We simplify the non-DMI part of the Hamiltonian based on the approach in Ref. [38] by introducing the following identities: $2\vec{m}_i\vec{m}_{i+1} = \vec{m}_i^2 + \vec{m}_{i+1} - (\vec{m}_{i+1} - \vec{m}_i)^2$ and $(\vec{l}_i\vec{m}_{i+1} - \vec{m}_i\vec{l}_{i+1}) = \vec{l}_i(\vec{m}_{i+1} - \vec{m}_i) - \vec{m}_i(\vec{l}_{i+1} - \vec{l}_i)$. The simplification of the DMI term is included in Appendix B. It is useful make a continuum approximation, $\vec{m}_{i+1} \approx \vec{m}_i + a_0(\partial\vec{m}_i/\partial z) + \cdots$ and $\vec{l}_{i+1} \approx \vec{l}_i + a_0(\partial\vec{l}_i/\partial z) + \cdots$, where a_0 is the lattice constant. In Eq. (1), we replace $\vec{m}_i$ and $\vec{l}_i$ by $\vec{m}(z)$ and $\vec{l}(z)$, respectively, and the sums are replaced by integrals. We describe the dynamics of the AFM in the exchange approximation and consider a slowly varying AFM domain wall. In this description, the exchange interaction is much larger than the anisotropic terms and $|\vec{m}|^2 \ll |\vec{l}|^2$. Thus the anisotropic terms proportional to the total magnetization can be neglected [38,50] (details are provided in Appendix A). Adding the DMI term, our expression in the continuum model is similar to that in Ref. [24]:

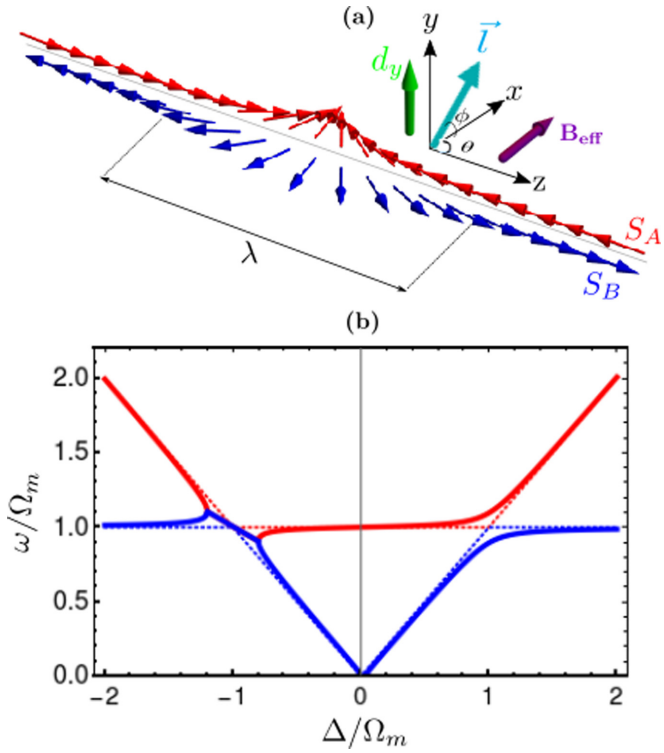

FIG. 1. (a) Schematic illustration of the geometry where the effective magnetic field of the light along $\hat{x}$ interacts with the domain wall with width λ and axis along $\hat{z}$ in the presence of DMI along $\hat{y}$. (b) Hybridized frequency of the cavity modes and magnon modes of the antiferromagnetic domain wall as a function of the detuning parameter in the absence of DMI. In the absence of DMI, there is no coupling achieved as indicated by the dotted lines. The thick lines represent what happens in the presence of DMI when the magnon modes couple to the cavity modes. The real part of the two modes attract in the region of negative detuning and repulsion is observed in the region of positive detuning.

$$\mathcal{H}_{\rm dw} = \int_{-\infty}^{\infty}\frac{dz}{a_0}\left[\frac{a}{2}|\vec{m}|^2 + \frac{A}{2}\left|\frac{\partial\vec{l}}{\partial z}\right|^2 + L\left(\vec{m}\cdot\frac{\partial\vec{l}}{\partial z}\right) - \frac{k_z}{2}(\vec{l}\cdot\hat{z})^2 - \frac{k_x}{2}(\vec{l}\cdot\hat{x})^2 + \vec{d}\cdot\left(\frac{\partial\vec{l}}{\partial z}\times\vec{l}\right) + \vec{d}_0\cdot(\vec{m}\times\vec{l})\right], \quad (2)$$

where $a = 8JS^2$ and $A = a_0^2JS^2$ are the homogeneous and nonhomogeneous exchange constants, respectively, $L = 2a_0JS^2$ is the parity-breaking term [24,38], the anisotropies are $k_z = 2K_zS^2$ and $k_x = 2K_xS^2$, and the DMI coefficients are $\vec{d} = a_0S^2\vec{D}$ and $\vec{d}_0 = 4S^2\vec{D}$.

The Lagrangian of the system, $\mathcal{L} = \mathcal{L}_B - \mathcal{H}_{\rm dw}$, is constructed using the Berry phase, $\mathcal{L}_B = 2\hbar S\,\vec{m}(\partial_t\vec{l}\times\vec{l})$ [24,38,40], which accounts for the inertia of the antiferromagnetic domain wall. By varying the Lagrangian with respect to $\vec{m}$, we derive an expression for $\vec{m}$ in terms of the temporal and

spatial derivative of $\vec{l}$:

$$\vec{m} = \frac{\rho}{a}\left(\vec{l} \times \frac{\partial \vec{l}}{\partial t}\right) - \frac{L}{a}\left(\frac{\partial \vec{l}}{\partial z}\right) + \frac{1}{a}\vec{d}_0 \times \vec{l}, \tag{3}$$

where $\rho = 2\hbar S$. Equation (3), which implies that $\vec{m}$ is a slave variable to $\vec{l}$ [24,38], is substituted into Eq. (2), making it possible to eliminate $\vec{m}$ from Eq. (2). We simplify Eq. (2) and disregard the total time derivatives proportional to the homogeneous DMI and terms proportional to the topological term, L, that do not contribute to the equations of motion [24] (see Appendix A for details). The Hamiltonian is thus

$$\mathcal{H}_{\rm dw} = \int_{-\infty}^{\infty} \frac{dz}{a_0}\left[\frac{\rho^2}{2a}\left(\frac{\partial \vec{l}}{\partial t}\right)^2 + \frac{A}{2}\left|\frac{\partial \vec{l}}{\partial z}\right|^2 - \frac{k_z}{2}(\vec{l}\cdot\hat{z})^2 - \frac{k_x}{2}(\vec{l}\cdot\hat{x})^2 + \vec{d}\cdot\left(\frac{\partial \vec{l}}{\partial z} \times \vec{l}\right)\right]. \tag{4}$$

We parametrize the staggered magnetization $\vec{l}$ by polar and azimuthal angles θ and ϕ in spherical coordinates: $\vec{l} = (\sin\theta\ \cos\phi, \sin\theta\ \sin\phi, \cos\theta)$. For the static wall configuration, $\partial\vec{l}/\partial t = 0$ in Eq. (4). By this definition, the Hamiltonian of the system is

$$\mathcal{H}_{\rm dw} = \int_{-\infty}^{\infty} \frac{dz}{a_0}\left[A\left(\frac{\partial\theta}{\partial z}\right)^2 - k_x \sin^2\theta\ \cos^2\phi - k_z\cos^2\theta - d_x\left(\frac{\partial\theta}{\partial z}\right)\sin\phi + d_y\left(\frac{\partial\theta}{\partial z}\right)\cos\phi\right], \tag{5}$$

where d_x and d_y are the x and y components of the DMI, respectively. The domain wall static profile is obtained using standard methods [38,46,49,51,52]. The domain wall tilt angle is defined as ϕ with respect to the x-z plane and assumed to be constant throughout the wall [46]. The energy density is minimized via the Euler-Lagrange equation giving a wall profile $\theta(z) = 2\tan^{-1}\exp[(z - z_0)/\lambda]$, where $\lambda = \sqrt{A/(k_z - k_x\cos^2\phi)}$ is the characteristic domain wall width. Our analysis of the static wall profile dependence on DMI agrees with the results in Ref. [46]. We summarize the key details in subsequent paragraphs.

The wall energy $\mathcal{E} = 4\sqrt{A(k_z - k_x\cos^2\phi)} - d_x\pi\ \sin\phi + d_y\pi\ \cos\phi$ is obtained by substituting the wall profile into Eq. (5) and integrating with respect to z. Since the energy density depends on only the x and y components of the DMI, two DMI directions are considered. When coupling the domain wall to the cavity modes, we find that the direction of photon propagation must be perpendicular to both the DMI and the domain wall axis (z axis) in order for coupling to be achieved. This requires two possible geometries be considered.

First, DMI is considered to be present in the $\hat{x}$ direction. This results in a distortion of the spin orientation on the sublattices and consequently results in a DMI-dependent tilt angle [46],

$$\phi(d_x) = \mathrm{sgn}\, d_x \cdot \cos^{-1}\left(\pm\sqrt{\frac{(8Jk_x^2 - d_x^2 k_z\pi^2)}{(8Jk_x^2 - d_x^2 k_x\pi^2)}}\right), \tag{6}$$

which minimizes the energy density. This dependence remains valid until a saturated DMI strength of $d_{x,\rm sat} = 4/\pi\sqrt{Jk_x^2/2k_z}$ is reached beyond which $\phi(d_x) = \pi/2$.

For the second geometry where DMI is present along $\hat{y}$, the DMI breaks the degeneracy of the domain wall energy minima and favors one chirality of the wall at a critical value, $d_{y,\rm c} = 4k_x/\pi\sqrt{J/2(k_z - k_x)}$. The tilt angle $\phi(d_y) = 0$ if $d_y < d_{y,\rm c}$. Otherwise, $\phi(d_y) = \pi$.

III. DOMAIN WALL DYNAMICS

We discuss the effects of DMI on the dynamics of an antiferromagnetic domain wall when coupled to optical photons in an electromagnetic cavity. The dynamics of the antiferromagnet is described in the semiclassical approximation. For this purpose, the Lagrangian of the system is $\mathcal{L} = \mathcal{L}_B - \mathcal{H}_{\rm dw}$ [24], where the first term corresponds to the Berry phase [24,38,40] and the second term is the magnetic energy in Eq. (5). We describe the domain wall dynamics using the collective coordinate method [35,53], treating the position of the domain wall $Z_0(t)$ as a dynamical variable. The effective Lagrangian in terms of the domain wall position $Z_0(t)$ and small fluctuations around the domain wall profile, $\delta\theta(t)$, is obtained from Eq. (5) by performing the expansion $\phi(z,t) = \phi_0[z - Z_0(t)]$ and $\theta(z,t) = \theta_0[z - Z_0(t)] + \delta\theta[z - Z_0(t)]$. For the fluctuations $\delta\theta(t)$, we obtain the Pöschl-Teller equation. The solution is $\delta\theta = p(t)\,\mathrm{sech}\{[z - Z_0(t)]/\lambda\}$, where p is the amplitude of the out-of-plane component.

In order to fully describe the dynamics of the antiferromagnetic domain wall, we include a pinning potential. The pinning potential provides a restoring force and is introduced as a point defect which contributes to the anisotropy along $\hat{y}$ at $z = 0$. The pinning potential $V_{\rm pin} = -K_{\rm pin}\int[\frac{dz}{a_0}\delta(z)\sin^2\theta(z)\sin^2\phi(z)] \approx K_{\rm pin}\,Z_0^2/\lambda^2$. We proceed to construct the total Lagrangian of the system following the approach in Ref. [24]. The effective Lagrangian for the collective coordinate $Z_0(t)$ in addition to the pinning potential $\mathcal{L} = \mathcal{L}_B - \mathcal{H}_{\rm dw} - V_{\rm pin}$ is expressed below:

$$\mathcal{L} = \frac{1}{a_0}\left(\frac{2\rho^2}{a\lambda}\dot{Z}_0^2 - \frac{a_0 K_{\rm pin}}{\lambda^2}Z_0^2 - 2A\lambda + 2K_x\cos^2\phi - \pi\lambda d_x\sin\phi + \pi\lambda d_y\cos\phi\right). \tag{7}$$

We define the generalized momentum $P_z = \partial\mathcal{L}/\partial\dot{Z}_0 = (4\rho^2/a_0\lambda)$ and $\dot{Z}_0 = (a_0\lambda P_z)/(4\rho^2)$.

From the Lagrangian in Eq. (7), we transform to the Hamiltonian description. The Hamiltonian of the pinned domain wall, excluding terms that do not contribute to the equations of motion, can then be written in terms of the wall position as

$$\mathcal{H}'_{\rm dw} = \frac{2\rho^2\dot{Z}_0^2}{a_0\,a\lambda} + \frac{K_{\rm pin}Z_0^2}{2}, \tag{8}$$

where we have dropped terms proportional to the out-of-plane component.

The Hamiltonian in Eq. (8) shows that the low energy motion of the pinned domain wall is similar to that of a massive particle in a parabolic potential. This motion can be quantized using a standard quantum-mechanical method of the quantization of a harmonic oscillator. From Eq. (8), we derive

the canonical conjugate momentum P_{Z_0} corresponding to Z_0, and the Hamiltonian is quantized by making the transformations $\hat{Z}_0 = \sqrt{\hbar/2M\Omega_m}(\hat{b} + \hat{b}^\dagger)$ and $\hat{P}_{Z_0} = -i\sqrt{\hbar M\Omega_m/2}(\hat{b} - \hat{b}^\dagger)$, where $\hat{b}$ and $\hat{b}^\dagger$ are the annihilation and the creation operators of the oscillator in Eq. (8), M is the domain wall effective mass, and Ω_m is the characteristic oscillation frequency of the domain wall.

The coupling mechanism between the domain wall and cavity photon is assumed to be the inverse Faraday effect [44]. In this way, the coupling appears as a reaction force to photon pressure exerted as compensation to changes in photon polarization. Details can be found in Refs. [23,43,54–56]. The magneto-optical interaction energy [56] is expressed as

$$\mathcal{H}_{\rm mo} = -\frac{i}{4} f\epsilon_0 \int d^3r\, \vec{m}(\vec{r}) \cdot [\vec{E}^*(\vec{r},t) \times \vec{E}(\vec{r},t)], \quad (9)$$

where $\vec{m}$ is the total magnetization vector, f is the Faraday rotation material-dependent parameter, ϵ_0 is the permittivity of free space, and $\vec{E}$ is the electric field vector of light. In this work, $\vec{m}$ is given by Eq. (3).

The first of the two geometries considered is that in which there is an electromagnetic wave propagating along $\hat{x}$ and circularly polarized in the y-z plane. In this geometry, the resulting effective magnetic field of light in Eq. (9) is given by $\vec{E}^*(x) \times \vec{E}(x) = \hat{x}\,(i\hbar\omega)/(2V\epsilon_0)[\hat{a}_R^\dagger \hat{a}_R - \hat{a}_L^\dagger \hat{a}_L]$, where V is the volume of the cavity and $\hat{a}_{R(L)}$ is related to the right (left) circularly polarized basis. The magneto-optical Hamiltonian obtained from Eq. (9), considering only the right-circular polarization, is $\mathcal{H}_{\rm mo}^x = (-if/4)(A_\perp/2V)[(-\rho/a)\sin\phi \dot{Z}_0 + (2d_y/a)Z_0]\hbar\omega_c \hat{a}_R^\dagger \hat{a}_R$, where $A_\perp$ is the sample cross section. This shows that the interaction along $\hat{x}$ is proportional to the tilt angle of the domain wall and the y component of the DMI (perpendicular to both the wall axis and the direction of propagation of electromagnetic waves).

In addition, we introduce the photonic Hamiltonian $\mathcal{H}_{\rm ph} = \hbar\omega_c \hat{a}^\dagger \hat{a}$ and an external laser driving term $\mathcal{H}_{\rm drive} = \varepsilon \hat{a}^\dagger e^{-i\omega_d t} + \varepsilon^* \hat{a}\, e^{i\omega_d t}$, where ε is the pump amplitude and ω_d is the driving frequency. In order to remove the time dependence of the driving terms, we move to a rotating frame defined by the cavity field photon number, rotating at a drive frequency ω_d by performing the unitary transformation $\mathcal{H}'_{\rm (ph,drive)} = -i\hbar(d\hat{U}^\dagger/dt)\hat{U} + \hat{U}\,(\mathcal{H}_{\rm drive} + \mathcal{H}_{\rm ph})\,U^\dagger$, where $\hat{U}(t) = e^{i\hbar\omega_d t \hat{a}^\dagger \hat{a}}$ [4]. This gives $\mathcal{H}'_{\rm (ph,drive)} = -\hbar\Delta\hat{a}^\dagger\hat{a} + \varepsilon\hat{a}^\dagger + \varepsilon^*\hat{a}$, where $\Delta = \omega_d - \omega_c$ is the laser detuning parameter. The effective Hamiltonian of the system is

$$\mathcal{H}_{\rm tot} = \hbar\Omega_m \hat{b}^\dagger\hat{b} - \hbar\Delta\hat{a}^\dagger\hat{a} + \varepsilon\hat{a}^\dagger + \varepsilon^*\hat{a} - \hbar g_0\left(-i\sin\phi\frac{\hbar\Omega_m}{K_z}(\hat{b}-\hat{b}^\dagger) + \frac{2d_y}{a}(\hat{b}+\hat{b}^\dagger)\right)\hbar\omega_c \hat{a}_{\rm R}^\dagger \hat{a}_{\rm R}, \quad (10)$$

where $g_0 = \frac{1}{4} f S_{\rm eff}\omega_c$. $S_{\rm eff} = A_\perp x_{\rm zpf}/V$, where $A_\perp$ is the sample cross section, V is the volume of the cavity, and $x_{\rm zpf} = \sqrt{\hbar/(2M\Omega_m)}$. $f = 2c\theta_f\sqrt{\epsilon}/\omega_c$ is the Faraday rotation per length, c is the speed of light in vacuum, and ϵ is the dieletric constant of the material. The antiferromagnetic domain wall effective mass is $M = 4\hbar^2/(a_0 K_z \lambda)$ and the characteristic oscillation frequency $\Omega_m = \sqrt{K_{\rm pin}/(M\lambda^2)}$.

As an example, we estimate values for a common antiferromagnet using experimental data for NiO having a domain wall width of approximately 150 nm [23], $a_0 = 0.418$ nm [57], and $K_z = 4$ K$/k_B$ [58], where k_B is the Boltzmann constant. We assume $K_{\rm pin} = 1$ K$/k_B$ such that it is of the same order of magnitude as the anisotropy constant. This gives $M \approx 10^{-29}$ kg and $\Omega_m \approx 10$ GHz. Due to the lack of experimental data on optomagnonic coupling with AFMs, we assume a material size similar to a YIG sphere of diameter 0.25 mm in a cavity having a dimension of $40 \times 25 \times 15$ mm^3 [17], such that $S_{\rm eff} \approx 10^{-10}$, $\epsilon = 5$, and $\theta_f = 419$ rad m^{-1} [1,59,60]. We estimate the coupling strength in Eq. (10) as $g_0 = c\theta_f\sqrt{\epsilon}S_{\rm eff}/2 \approx 40.7$ Hz.

The equations of motion for $\hat{a}$, $\hat{a}^\dagger$, $\hat{b}$, and $\hat{b}^\dagger$ in the Appendixes are obtained from Eq. (10) and linearized by splitting the operators into an average plus a fluctuating term, e.g., $\hat{a} = \langle\hat{a}\rangle + \delta\hat{a}$, where $\langle\hat{a}\rangle$ is related to the average number of cavity photons, $\bar{n}_c = |\langle\hat{a}\rangle|^2$ [4]. Solving the equations of motion for the hybridized frequency ω, we obtain two pairs of

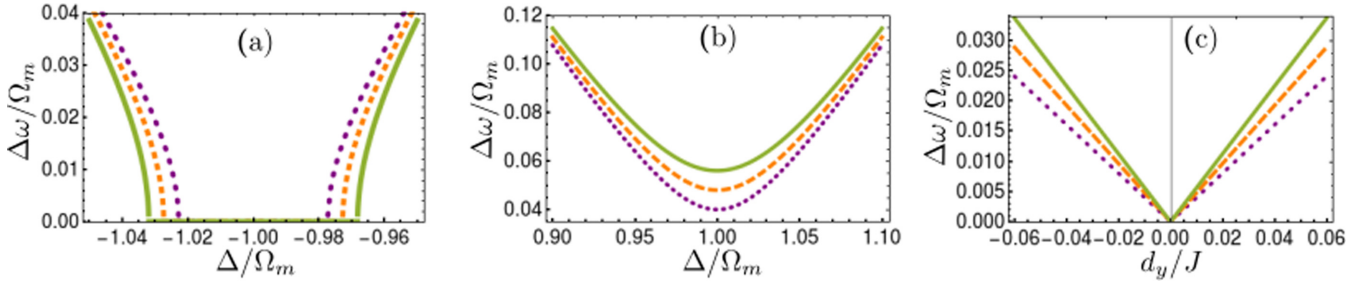

FIG. 2. (a) Frequency gap in the presence of DMI of strength $0.06J$ as a function of the negative detuning around the point of attraction for different coupling strengths: $g = 0.10$ MHz, $g = 0.12$ MHz, and $g = 0.14$ MHz represented by the purple dotted, orange dashed, and green solid lines, respectively. Around the exceptional point, attraction dominates a wider range for larger coupling strengths and decreases for lower coupling strengths. (b) Frequency gap in the presence of DMI of strength $0.06J$ as a function of the positive detuning. For the same value of detuning, larger frequency gaps are observed for larger coupling. In all cases, the gap is minimum at resonance and increases as we move away from resonance. (c) Frequency gap as a function of negative and positive DMI present along the $\hat{y}$. At $d_y = 0$ there is no gap. In the presence of DMI, the frequency gaps increase linearly with increasing magnitude of DMI and the gap is observed to be larger for larger coupling strengths.

eigenmodes:

$$\omega_{\pm} = \sqrt{\frac{\Delta^2 + \Omega_m^2}{2} \pm \sqrt{\frac{\left(\Delta^2 - \Omega_m^2\right)^2}{4} - 16g^2\tilde{d}_y^2\Delta\Omega_m}}, \quad (11)$$

where $\tilde{d}_y = d_y/a$ and $g = \sqrt{\bar{n}_c}g_0$ is the measure of the photon-enhanced coupling of magnons to photonic modes. $g \approx 0.1$–1 MHz for a microcavity that can support up to 10^7–10^9 photons [1]. Equation (11) shows that, if there was no coupling (i.e., $g = 0$), there would be crossing of the modes. The same result is realized in the absence of DMI since $d_y = 0$ and $\phi(d_y) = 0$ do not provide coupling in Eq. (11). The dotted lines in Fig. 1(b) show crossing of modes in both regions ($\Delta > 0$ and $\Delta < 0$) when DMI is absent, and no coupling is evident. The thick lines show that, in the presence of DMI, degeneracy is broken and avoided crossing of modes is realized for positive detuning ($\Delta > 0$), indicating coherent coupling of the modes. In the region of negative detuning ($\Delta < 0$), there are exceptional points where the eigenfrequencies become complex and there is coalescence of their real parts resulting in mode attraction.

In order to illustrate the consequence of the presence of DMI on resonances, we study the frequency gaps, $\Delta\omega = \omega_+ - \omega_-$. In Fig. 2, $\Delta\omega$ is shown as a function of Δ for different values of g. In the region of negative detuning [Fig. 2(a)], around the exceptional points, there is no frequency gap and the attraction regime spans a wider range of detuning for increasing coupling strengths. Away from the exceptional points we observe a difference in frequencies of the two modes. On the other hand, in the region of repulsion [Fig. 2(b)], there exists a frequency gap. This gap can be seen to increase with increasing coupling strength. Figure 2(c) provides a description of how frequency gaps for positive and negative Δ depend on DMI at resonance. The gaps increase with increasing magnitude of DMI and vanish in the absence of DMI. We conclude that the coupling of the photonic mode to the magnonic mode is dependent on the DMI strength.

The second geometry considered in this work is the case where the domain wall interacts with waves propagating along $\hat{y}$ and circularly polarized in the x-z plane [Fig. 3(a)]. In this geometry, the coupling of cavity modes to the domain wall excitations is realized even in the absence of DMI. We observe that this coupling is stronger than in the first geometry considered due to the fact that the electromagnetic wave is applied in a direction perpendicular to the easy plane of the domain wall, thus maximizing coupling to the variation of magnetization. Following a similar approach described for the first geometry considered, we obtain two pairs of eigenmodes:

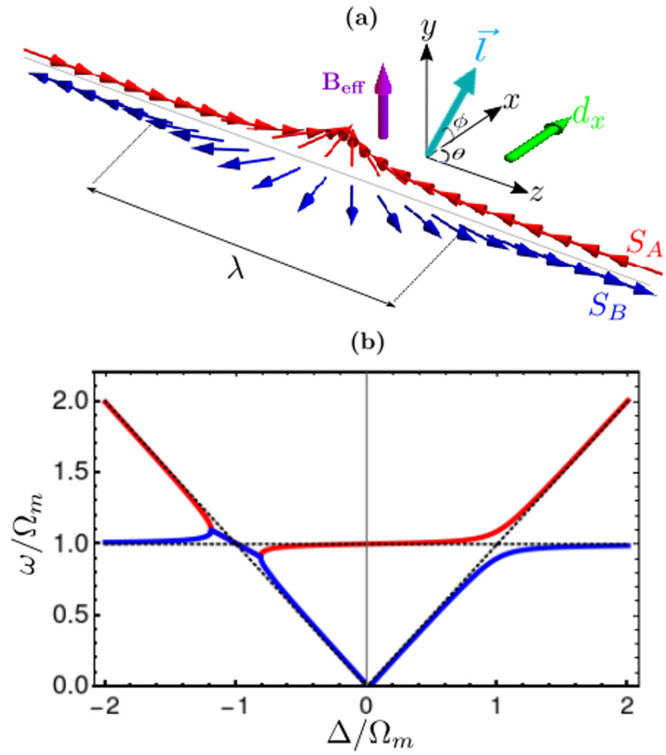

FIG. 3. (a) Schematic illustrating the geometry where the effective magnetic field of the light along $\hat{y}$ interacts with the domain wall of width, λ with axis along $\hat{z}$ in the presence of DMI along $\hat{x}$. (b) Hybridized frequency of the cavity modes and magnon modes of the antiferromagnetic domain wall as a function of the detuning parameter in the absence of DMI. The red and blue thick lines indicate coupling between the magnonic and photonic modes in the absence of DMI. The real part of the two modes attract in the region of negative detuning and repulsion is observed in the region of positive detuning. As the magnitude of DMI increases, coupling between modes reduces until no coupling is achieved. The black dotted lines show that there is no coupling at the saturated value of DMI.

$$\omega_{\pm} = \sqrt{\frac{\Delta^2 + \Omega_m^2}{2} \pm \sqrt{\frac{\left(\Delta^2 - \Omega_m^2\right)^2}{4} - 16g^2\tilde{d}_x^2\Delta\Omega_m - 2g^2\pi^2\Delta\Omega(1 + \cos 2\phi)}}, \quad (12)$$

where $\tilde{d}_x = d/a$. Figure 3(b) shows a plot of the hybridized frequency in Eq. (12) as a function of the detuning parameter, Δ.

We discuss what happens when DMI is absent ($d_x = 0$). The thick red and blue lines in Fig. 3(b) indicate that there is coupling even in the absence of DMI. However, when DMI is present along $\hat{x}$, the spin orientations are distorted out of the plane of the wall and we have a nonzero tilt angle which depends on the DMI strength. This modifies the domain wall width as $\lambda_{d_x} = \sqrt{A/[k_z - k_x(8Jk_x^2 - d_x^2k_z\pi^2)/(8Jk_x^2 - d_x^2k_x\pi^2)]}$. The consequence of this is a weaker magneto-optical coupling in the interaction for both positive and negative values of DMI and symmetric about $d_x = 0$ up to the saturated value $d_{sat} = 4/\pi\sqrt{Jk_x^2/2k_z}$ (when crossing of the modes emerges in both regions). As indicated by the black dotted lines in Fig. 3(b),

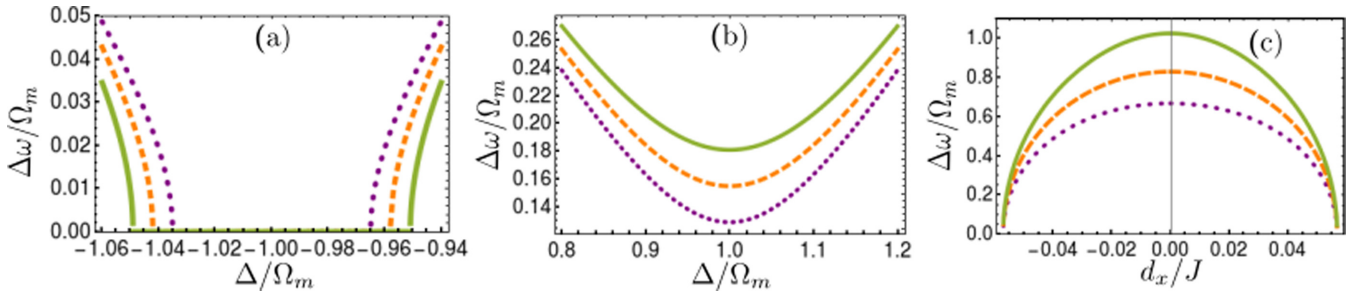

FIG. 4. Effect of DMI of strength $0.06J$ on the frequency gaps as (a) a function of the negative detuning around the point of attraction for different coupling strengths: $g = 0.10$ MHz, $g = 0.12$ MHz, and $g = 0.14$ MHz represented by the purple dotted, orange dashed, and green solid lines, respectively. Around the exceptional point, attraction dominates a wider range for larger coupling strengths and decreases for lower coupling strengths. (b) Frequency gap in the presence of DMI of strength $0.06J$ as a function of the positive detuning. For the same value of detuning, larger frequency gaps are observed for larger coupling. In all cases, the gap is minimum at resonance and increases as we move away from resonance. (c) Frequency gap as a function of negative and positive DMI present along the $\hat{y}$. The values of the coupling strength g become more important as d_x approaches zero. The frequency gap reduces for increasing magnitude of the DMI and vanishes as the saturated value of DMI is reached.

DMI reduces the coupling strength between the modes until crossing of the mode is achieved just as $d_x = d_{\text{sat}}$.

The dependence of the frequency gaps on the detuning in the presence of DMI along x is similar to what we observed along y except that the attraction and repulsion are stronger for the same value of DMI if we compare Figs. 2(a) and 2(b) to Figs. 4(a) and 4(b). The most striking feature that distinguishes both geometries is how the frequencies change with respect to the DMI. Contrary to the previous geometry, increase in the DMI applied along x leads to decrease in the frequencies until the gap vanishes at the saturated value of DMI [Fig. 4(c)]. It is useful to define the frequency gap $\Delta\omega(\tilde{d}_x)$ in order to see clearly how the frequency gap depends on DMI at resonance. We calculate this from Eq. (12): $\Delta\omega(d_x) = \omega_+ - \omega_-|_{\Omega_m=\Delta=1} \approx 2g\{8\tilde{d}_x^2 + \pi^2[1 + \cos 2\phi(\tilde{d}_x)]\}$. For example, if we assume a coupling strength of 0.1 MHz at a tilt angle of $\pi/2$, then $\Delta\omega \approx 2\tilde{d}_x^2$ MHz. This shows that the gap depends on the DMI constant and may be used to determine the DMI strength for given values of the coupling strength.

IV. CONCLUSION

We demonstrated that the collective excitation of a Neél antiferromagnetic domain wall can be realized through magneto-optical coupling to cavity photons. The resulting Hamiltonian is of an optomagnonic type, which allows realization of optomechanical instabilities such as level attraction in a driven system. We find that the presence of DMI enables coupling between a domain wall and cavity photons in a geometry where there is no coupling otherwise. This opens a possibility for estimating DMI in antiferromagnetic materials by measuring the interaction of antiferromagnetic resonances to optical modes in an optical cavity. This approach is not limited to a single domain wall dynamics but applicable to other one-dimensional textures like chiral soliton lattice in ferromagnets and antiferromagnets and can, in principle, be extended to antiferromagnetic spin textures in two spatial dimensions such as skyrmions and skyrmion lattices, which remains a future problem.

ACKNOWLEDGMENTS

This work was supported by The Natural Sciences and Engineering Research Council of Canada (NSERC) Discovery, John R. Leaders Fund–Canada Foundation for Innovation (CFI-JELF), Research Manitoba and the University of Manitoba, Canada.

APPENDIX A

1. Domain wall configuration

Our model begins with a one-dimensional (1D) Heisenberg antiferromagnetic chain, which contains an even number of lattice sites. The 1D AFM chain can be described by the Hamiltonian which comprises the exchange coupling between spin vectors on two sublattices and uniaxial anisotropies in the $\hat{z}$ and $\hat{x}$ directions:

$$\mathcal{W} = \sum_{i=0}^{2N-1} [J\vec{S}_i \cdot \vec{S}_{i+1} - K_x(\vec{S}_{i,x}) - K_z(\vec{S}_{i,z})]. \tag{A1}$$

We split the chain into lattice cells with sublattices A and B:

$$\mathcal{W} = \sum_{i=0}^{N-1} \left[J\left(\vec{S}_A^i \cdot \vec{S}_B^i + \vec{S}_B^i \cdot \vec{S}_A^{i+1}\right) - \frac{K_x}{2}\left(\left(\vec{S}_A^i \cdot \hat{x}\right)^2 + \left(\vec{S}_B^i \cdot \hat{x}\right)^2\right) - \frac{K_z}{2}\left(\left(\vec{S}_A^i \cdot \hat{z}\right)^2 + \left(\vec{S}_B^i \cdot \hat{z}\right)^2\right)\right]. \tag{A2}$$

Next, we define the total magnetization $\vec{m}_i$ and staggered magnetization $\vec{l}_i$ of the sublattices, respectively, as

$$\vec{m}_i = \frac{\vec{S}_A^i + \vec{S}_B^i}{2S}, \tag{A3a}$$

$$\vec{l}_i = \frac{\vec{S}_A^i - \vec{S}_B^i}{2S}, \tag{A3b}$$

subject to the constraints $\vec{m} \cdot \vec{l} = 0$ and $\vec{m}^2 + \vec{l}^2 = 1$.

From Eqs. (A3a) and (A3b),

$$\vec{S}_A^i = S(\vec{m}_i + \vec{l}_i), \tag{A4a}$$

$$\vec{S}_B^i = S(\vec{m}_i - \vec{l}_i). \tag{A4b}$$

By substituting Eqs. (A4a) and (A4b) into Eq. (A2), the Hamiltonian reduces to a sum over the antiferromagnetic lattice points and no longer sums over spins:

$$\mathcal{W} = \sum_{i=0}^{N-1} \left[JS^2((\vec{m}_i + \vec{l}_i)(\vec{m}_i - \vec{l}_i) + (\vec{m}_i - \vec{l}_i)(\vec{m}_{i+1} + \vec{l}_{i+1})) - \frac{K_x S^2}{2}\left((\vec{m}_i + \vec{l}_i)_x^2 + (\vec{m}_i - \vec{l}_i)_x^2\right) - \frac{K_z S^2}{2}\left((\vec{m}_i + \vec{l}_i)_x^2 + (\vec{m}_i - \vec{l}_i)_z^2\right) \right], \tag{A5}$$

$$\mathcal{W} = \sum_{i=0}^{N-1} \{ JS^2(\vec{m}_i - \vec{l}_i)[(\vec{m}_i + \vec{l}_i) + (\vec{m}_{i+1} + \vec{l}_{i+1})] - K_x S^2[(m_{i,x})^2 + (l_{i,x})^2] - K_z S^2[(m_{i,z})^2 + (l_{i,z})^2] \}. \tag{A6}$$

We introduce the following identities to simplfy Eq. (A6) [38]:

$$2\vec{m}_i\vec{m}_{i+1} = \vec{m}_i^2 + (\vec{m}_{i+1})^2 - (\vec{m}_{i+1} - \vec{m}_i)^2, \tag{A7a}$$

$$\vec{m}_i\vec{l}_{i+1} - \vec{l}_i\vec{m}_{i+1} = \vec{m}_i(\vec{l}_{i+1} - \vec{l}_i) - \vec{l}_i(\vec{m}_{i+1} - \vec{m}_i). \tag{A7b}$$

Substituting (A7a) and (A7b) into (A6) and working through the algebra carefully, we arrive at

$$\mathcal{W} = \sum_{i=0}^{N-1} \left\{ JS^2 \left[2\left(\vec{m}_i^2 - \vec{l}_i^2\right) + \vec{m}_i(\vec{l}_{i+1} - \vec{l}_i) - \vec{l}_i(\vec{m}_{i+1} - \vec{m}_i) + \frac{1}{2}[(\vec{l}_{i+1} - \vec{l}_i)^2 - (\vec{m}_{i+1} - \vec{m}_i)^2] \right] \right.$$
$$\left. - K_x S^2\left(\vec{m}_{i,x}^2 + \vec{l}_{i,x}^2\right) - K_z S^2\left(\vec{m}_{i,z}^2 + \vec{l}_{i,z}^2\right) \right\}. \tag{A8}$$

We move to the continuum model:

$$\mathcal{W} = \sum_{i=0}^{N-1} \left\{ JS^2 \left[2\left(\vec{m}_i^2 - \vec{l}_i^2\right) + \left(\vec{m}_i \frac{\partial \vec{l}_i}{\partial z} - \vec{l}_i \frac{\partial \vec{m}_i}{\partial z}\right) a_0 + \frac{a_0^2}{2}\left(\left(\frac{\partial \vec{l}_i}{\partial z}\right)^2 - \left(\frac{\partial \vec{m}_i}{\partial z}\right)^2\right) \right] - K_x S^2\left(\vec{m}_{i,x}^2 + \vec{l}_{i,x}^2\right) - K_z S^2\left(\vec{m}_{i,z}^2 + \vec{l}_{i,z}^2\right) \right\}, \tag{A9}$$

where a_0 is the length of the antiferromagnetic unit cell and is equal to twice the nearest neighbor spacing in the linear chain. Converting the sums to integrals,

$$\mathcal{W} = \int_0^{L_z} \frac{dz}{a_0} \left\{ 2JS^2(\vec{m}^2 - \vec{l}^2) + JS^2 a_0 \left[\vec{m} \cdot \frac{\partial \vec{l}}{\partial z} - \vec{l} \cdot \frac{\partial \vec{m}}{\partial z} \right] + JS^2 a_0^2 \left[\left(\frac{\partial \vec{l}}{\partial z}\right)^2 + \left(\frac{\partial \vec{m}}{\partial z}\right)^2 \right] \right.$$
$$\left. - K_x S^2[(\vec{m} \cdot \hat{x})^2 + (\vec{l} \cdot \hat{x})^2] - K_z S^2[(\vec{m} \cdot \hat{z})^2 + (\vec{l} \cdot \hat{z})^2] \right\}. \tag{A10}$$

Using the constraints $\vec{m} \cdot \vec{l} = 0$ and $\vec{m}^2 + \vec{l}^2 = 1$, which give $\vec{l}^2 = 1 - \vec{m}^2$, and recognizing that $\frac{\partial}{\partial z}(\vec{m} \cdot \vec{l}) = \vec{m} \cdot \frac{\partial \vec{l}}{\partial z} + \vec{l} \cdot \frac{\partial \vec{m}}{\partial z}$ leads to $\vec{m} \cdot \frac{\partial \vec{l}}{\partial z} = -\vec{l} \cdot \frac{\partial \vec{m}}{\partial z}$. The energy thus becomes

$$\mathcal{W} = \int_{-\infty}^{\infty} \frac{dz}{a_0} \left\{ \frac{a}{2}|\vec{m}|^2 + \frac{A}{2}\left[\left(\frac{\partial \vec{m}}{\partial z}\right)^2 + \left(\frac{\partial \vec{l}}{\partial z}\right)^2 \right] + L\left(\vec{m} \cdot \frac{\partial \vec{l}}{\partial z}\right) - \frac{k_x}{2}[(\vec{m} \cdot \hat{x})^2 + (\vec{l} \cdot \hat{x})^2] - \frac{k_z}{2}[(\vec{m} \cdot \hat{z})^2 + (\vec{l} \cdot \hat{z})^2] \right\}, \tag{A11}$$

where $a = 8JS^2$ and $A = a_0^2 JS^2$ are the homogeneous and nonhomogeneous exchange constants, respectively, $L = 2a_0 JS^2$ is the parity-breaking term [24,38], and the anisotropies are $k_z = 2K_z S^2$ and $k_x = 2K_x S^2$. We describe the dynamics of the AFM in the exchange approximation ($J \gg K$) and also consider the slowly varying AFM domain wall in our description of the staggered

magnetization such that $|\vec{m}|^2 \ll |\vec{l}|^2$. In this approximation, $(\partial\vec{m}/\partial z)^2 = (\vec{m}^2/\vec{l}^2)(\partial\vec{l}/\partial z)^2 \to 0$ and we neglect the anisotropic terms proportional to $(\vec{m}\cdot\hat{x})^2$ and $(\vec{m}\cdot\hat{z})^2$. We arrive at

$$\mathcal{W} = \int_{-\infty}^{\infty} \frac{dz}{a_0}\left[\frac{a}{2}|\vec{m}|^2 + \frac{A}{2}\left|\frac{\partial\vec{l}}{\partial z}\right|^2 + L\left(\vec{m}\cdot\frac{\partial\vec{l}}{\partial z}\right) - \frac{k_x}{2}(\vec{l}\cdot\hat{x})^2 - \frac{k_z}{2}(\vec{l}\cdot\hat{z})^2\right], \tag{A12}$$

which when combined with the DMI terms gives Eq. (2) in the main text:

$$\mathcal{H}_{\rm dw} = \int_{-\infty}^{\infty} \frac{dz}{a_0}\left[\frac{a}{2}|\vec{m}|^2 + \frac{A}{2}\left|\frac{\partial\vec{l}}{\partial z}\right|^2 + L\left(\vec{m}\cdot\frac{\partial\vec{l}}{\partial z}\right) - \frac{k_z}{2}(\vec{l}\cdot\hat{z})^2 - \frac{k_x}{2}(\vec{l}\cdot\hat{x})^2 + \vec{d}\cdot\left(\frac{\partial\vec{l}}{\partial z}\times\vec{l}\right) + \vec{d}_0\cdot(\vec{m}\times\vec{l})\right]. \tag{A13}$$

Having obtained the Hamiltonian of the system, we proceed to derive the Lagrangian for the system by introducing the Berry phase term: $\mathcal{L}_{\rm B} = 2\hbar S\vec{m}(\partial\vec{l}/\partial t\times\vec{l})$. The Lagrangian $\mathcal{L} = \mathcal{L}_{\rm B} - \mathcal{H}_{\rm dw}$ is

$$\mathcal{L}_{\rm dw} = \int_{-\infty}^{\infty} \frac{dz}{a_0}\left[\rho\,\vec{m}\cdot\left(\vec{l}\times\frac{\partial\vec{l}}{\partial t}\right) - \frac{a}{2}|\vec{m}|^2 - \frac{A}{2}\left|\frac{\partial\vec{l}}{\partial z}\right|^2 - L\left(\vec{m}\cdot\frac{\partial\vec{l}}{\partial z}\right) + \frac{k_z}{2}(\vec{l}\cdot\hat{z})^2 + \frac{k_x}{2}(\vec{l}\cdot\hat{x})^2 - \vec{d}\cdot\left(\frac{\partial\vec{l}}{\partial z}\times\vec{l}\right) - \vec{d}_0\cdot(\vec{m}\times\vec{l})\right], \tag{A14}$$

where $\rho = 2\hbar S$. We can exclude $\vec{m}$ from the Lagrangian by minimizing Eq. (A14) with respect to $\vec{m}$. The result of the minimization is given in Eq. (3) of the main text:

$$\vec{m} = \frac{\rho}{a}\left(\vec{l}\times\frac{\partial\vec{l}}{\partial t}\right) - \frac{L}{a}\left(\frac{\partial\vec{l}}{\partial z}\right) + \frac{1}{a}\vec{d}_0\times\vec{l}. \tag{A15}$$

Equation (3) implies that $\vec{m}$ is a slave variable to $\vec{l}$ [24,38]. Substituting this result into (A14) and simplifying, we obtain

$$\mathcal{L}_{\rm dw} = \int_{-\infty}^{\infty} \frac{dz}{a_0}\left[\frac{\rho^2}{2a}\left(\frac{\partial\vec{l}}{\partial t}\right)^2 + \frac{3}{2a}(\vec{d}_0\times\vec{l})^2 + \frac{\rho}{a}\left(\vec{l}\times\frac{\partial\vec{l}}{\partial t}\right)\cdot(\vec{l}\times\vec{d}_0) - \frac{A}{2}\left|\frac{\partial\vec{l}}{\partial z}\right|^2 + \frac{k_z}{2}(\vec{l}\cdot\hat{z})^2 + \frac{k_x}{2}(\vec{l}\cdot\hat{x})^2 - \vec{d}\cdot\left(\frac{\partial\vec{l}}{\partial z}\times\vec{l}\right)\right], \tag{A16}$$

where we have neglected terms proportional to the topological term, L. We recognize that $(\vec{d}_0\times\vec{l})^2 = d_0^2 l^2 - (\vec{d}_0\cdot\vec{l})^2 = \text{const} - (\vec{d}_0\cdot\vec{l})^2$, which will not contribute to the equations of motion. Also, we neglect the total derivatives associated with the homogeneous DMI as they do not contribute to the equations of motion [24]. This leaves us with a Lagrangian which has no dependence on the total magnetization, $\vec{m}$:

$$\mathcal{L}_{\rm dw} = \int_{-\infty}^{\infty} \frac{dz}{a_0}\left[\frac{\rho^2}{2a}\left(\frac{\partial\vec{l}}{\partial t}\right)^2 - \frac{A}{2}\left|\frac{\partial\vec{l}}{\partial z}\right|^2 + \frac{k_z}{2}(\vec{l}\cdot\hat{z})^2 + \frac{k_x}{2}(\vec{l}\cdot\hat{x})^2 - \vec{d}\cdot\left(\frac{\partial\vec{l}}{\partial z}\times\vec{l}\right)\right]. \tag{A17}$$

For the static configuration, we set $\partial\vec{l}/\partial t = 0$ and parametrize $\vec{l}$ by polar and azimuthal angles in spherical coordinates: $\vec{l} = (\sin\theta\,\cos\phi, \sin\theta\,\sin\phi, \cos\theta)$. The equivalent Hamiltonian of the system given by Eq. (5) in the main text is

$$\mathcal{H}_{\rm dw} = \int_{-\infty}^{\infty} \frac{dz}{a_0}\left[A\left(\frac{\partial\theta}{\partial z}\right)^2 - k_x\sin^2\theta\,\cos^2\phi - k_z\cos^2\theta - d_x\left(\frac{\partial\theta}{\partial z}\right)\sin\phi + d_y\left(\frac{\partial\theta}{\partial z}\right)\cos\phi\right]. \tag{A18}$$

APPENDIX B

1. Dzyalonshinskii-Moriya interaction (DMI)

The DMI between two atomic spins S_i and S_{i+1} can be expressed as a vector product formed by the magnetic moments S_i of two magnetic ions,

$$\mathcal{H}_{\rm DMI} = \sum_i (-1)^i \vec{D}\cdot(\vec{S}_i\times\vec{S}_{i+1}). \tag{B1}$$

When written in terms of the nearest neighboring spins on the sublattices, we have

$$\mathcal{H}_{\rm DMI} = \sum_n \vec{D}\cdot\left(\vec{S}_n^A\times\vec{S}_n^B\right) + \vec{D}\left(\vec{S}_{n+1}^A\times\vec{S}_n^B\right),$$

where $\vec{S}^A = \vec{m} + \vec{l}$ and $\vec{S}^B = \vec{m} - \vec{l}$. Substituting these into the previous expression and doing some lines of vector algebra, we arrive at the expression

$$\mathcal{H}_{\rm DMI} = \sum_n \{4\vec{D}S^2\cdot(\vec{m}_n\times\vec{l}_n) - \vec{D}S^2[\vec{m}_{n+1}\times\vec{m}_n - \vec{l}_{n+1}\times\vec{l}_n - (\vec{m}_{n+1} - \vec{m}_n)\times\vec{l}_n + (\vec{l}_{n+1} - \vec{l}_n)\times\vec{m}_n]\}.$$

In the continuum limit,

$$\mathcal{H}_{\mathrm{DMI}} = \int \frac{dz}{a_0}\left\{\vec{d}_0 \cdot (\vec{m}\times\vec{l}) - \left[\vec{d}\cdot\left(\frac{\partial\vec{m}}{\partial z}\times\vec{m}\right) - \vec{d}\cdot\left(\frac{\partial\vec{l}}{\partial z}\times\vec{l}\right) - \vec{d}\cdot\left(\frac{\partial\vec{m}}{\partial z}\times\vec{l}\right) + \vec{d}\cdot\left(\frac{\partial\vec{l}}{\partial z}\times\vec{m}\right)\right]\right\}, \tag{B2}$$

where $\vec{d}_0 = 4S^2\vec{D}$ and $\vec{d} = a_0 S^2\vec{D}$. Integrating by parts, we find that $\vec{d}\cdot(\frac{\partial\vec{m}}{\partial z}\times\vec{l}) = \vec{d}\cdot(\frac{\partial\vec{l}}{\partial z}\times\vec{m})$ and thus the last two terms cancel out. Neglecting the second term, we are arrive at

$$\mathcal{H}_{\mathrm{DMI}} = \int \frac{dz}{a_0}\left\{\vec{d}_0\cdot(\vec{m}\times\vec{l}) + \vec{d}\cdot\left(\frac{\partial\vec{l}}{\partial z}\times\vec{l}\right)\right\}. \tag{B3}$$

The Lagrangian of the system which includes the DMI term in Eq. (B3) is varied with respect to $\vec{m}$ to obtain an expression for $\vec{m}$ as a slave variable to $\vec{l}$ which depends on $\vec{d}_0$, $\vec{l}$, and the spatial and temporal derivatives of $\vec{l}$:

$$\vec{m} = \frac{\rho}{a}\left(\vec{l}\times\frac{\partial\vec{l}}{\partial t}\right) - \frac{L}{a}\left(\frac{\partial\vec{l}}{\partial z}\right) + \frac{1}{a}\vec{d}_0\times\vec{l}, \tag{B4}$$

where a is the homogeneous exchange constant.

2. DMI-dependent equations of motion

The equations of motion in the presence of DMI are given. First, we consider the case where electromagnetic waves propagating along $\hat{x}$ couple to the wall position with DMI present in the $\hat{y}$ direction. The equations of motion in frequency space

$$\begin{pmatrix} -i(\omega-\Omega_m) & 0 & -g(\pi\Omega_m\sin\phi - 2id_y) & -g(\pi\Omega_m\sin\phi - 2id_y) \\ 0 & -i(\omega+\Omega_m) & -g(\pi\Omega_m\sin\phi + 2id_y) & -g(\pi\Omega_m\sin\phi + 2id_y) \\ g(\pi\Omega_m\sin\phi + 2id_y) & -g(\pi\Omega_m\sin\phi - 2id_y) & -i(\omega-\Delta) & 0 \\ -g(\pi\Omega_m\sin\phi + 2id_y) & g(\pi\Omega_m\sin\phi - 2id_y) & 0 & -i(\omega+\Delta) \end{pmatrix}\begin{pmatrix}\hat{b}\\ \hat{b}^\dagger\\ \delta\hat{a}\\ \delta\hat{a}^\dagger\end{pmatrix} = \begin{pmatrix}0\\0\\-i\varepsilon\\ i\varepsilon^*\end{pmatrix}. \tag{B5}$$

In this configuration, the propagating wave is in the hard axis of the wall and results in no magneto-optical coupling. We found that, for DMI to play a role, it must be perpendicular to both the wall direction ($\hat{z}$) and the direction of propagating wave ($\hat{x}$). Therefore, we consider DMI present along $\hat{y}$. The presence of DMI breaks the degeneracy which occurs at resonance and allows for magneto-optical coupling which depends on the y component of the DMI vector.

The second geometry considered is the one in which an electromagnetic wave propagating along $\hat{y}$ couples to the wall position with DMI present in the $\hat{x}$ direction. The electromagnetic wave is circularly polarized in the easy plane of the domain wall. As a result, there is a strong coupling. The plot of hybridized frequency against the detuning parameter is shown in Fig. 3(b). We draw the conclusion that in this geometry, whether DMI is present or not, there is coupling of photons to magnons; however, the presence of DMI leads to modulation of the frequencies. The equation of motion is given in matrix form:

$$\begin{pmatrix} -i(\omega-\Omega_m) & 0 & g(\pi\Omega_m\cos\phi - 2id_x) & g(\pi\Omega_m\cos\phi - 2id_x) \\ 0 & -i(\omega+\Omega_m) & g(\pi\Omega_m\cos\phi + 2id_x) & g(\pi\Omega_m\cos\phi + 2id_x) \\ -g(\pi\Omega_m\cos\phi + 2id_x) & g(\pi\Omega_m\cos\phi - 2id_x) & -i(\omega-\Delta) & 0 \\ g(\pi\Omega_m\cos\phi + 2id_x) & -g(\pi\Omega_m\cos\phi - 2id_x) & 0 & -i(\omega+\Delta) \end{pmatrix}\begin{pmatrix}\hat{b}\\ \hat{b}^\dagger\\ \delta\hat{a}\\ \delta\hat{a}^\dagger\end{pmatrix} = \begin{pmatrix}0\\0\\-i\varepsilon\\ i\varepsilon^*\end{pmatrix}. \tag{B6}$$

[1] S. Viola Kusminskiy, H. X. Tang, and F. Marquardt, Coupled spin-light dynamics in cavity optomagnonics, Phys. Rev. A **94**, 033821 (2016).

[2] R. Hisatomi, A. Osada, Y. Tabuchi, T. Ishikawa, A. Noguchi, R. Yamazaki, K. Usami, and Y. Nakamura, Bidirectional conversion between microwave and light via ferromagnetic magnons, Phys. Rev. B **93**, 174427 (2016).

[3] A. D. Karenowska, A. V. Chumak, A. A. Serga, and B. Hillebrands, Magnon spintronics, in *Handbook of Spintronics*, edited by Y. Xu, D. D. Awschalom, and J. Nitta (Springer Netherlands, Dordrecht, 2014), pp. 1–38.

[4] M. Aspelmeyer, T. J. Kippenberg, and F. Marquardt, Cavity optomechanics, Rev. Mod. Phys **86**, 1391 (2014).

[5] N. Brahms and D. M. Stamper-Kurn, Spin optodynamics analog of cavity optomechanics, Phys. Rev. A **82**, 041804(R) (2010).

[6] W. D. Heiss, Exceptional points of non-hermitian operators, J. Phys. A: Math. Gen. **37**, 2455 (2004).

[7] V. L. Grigoryan, K. Shen, and K. Xia, Synchronized spin-photon coupling in a microwave cavity, Phys. Rev. B **98**, 024406 (2018).

[8] B. Bhoi, B. Kim, S.-H. Jang, J. Kim, J. Yang, Y.-J. Cho, and S.-K. Kim, Abnormal anticrossing effect in photon-magnon coupling, Phys. Rev. B **99**, 134426 (2019).

[9] M. Harder, Y. Yang, B. M. Yao, C. H. Yu, J. W. Rao, Y. S. Gui, R. L. Stamps, and C.-M. Hu, Level Attraction Due to

Dissipative Magnon-Photon Coupling, Phys. Rev. Lett. **121**, 137203 (2018).
[10] W. Yu, J. Wang, H. Y. Yuan, and J. Xiao, Prediction of Attractive Level Crossing via a Dissipative Mode, Phys. Rev. Lett. **123**, 227201 (2019).
[11] P.-C. Xu, J. W. Rao, Y. S. Gui, X. Jin, and C.-M. Hu, Cavity-mediated dissipative coupling of distant magnetic moments: Theory and experiment, Phys. Rev. B **100**, 094415 (2019).
[12] Y.-P. Wang and C.-M. Hu, Dissipative couplings in cavity magnonics, J. Appl. Phys. **127**, 130901 (2020).
[13] I. Proskurin, R. Macedo, and R. L. Stamps, Microscopic origin of level attraction for a coupled magnon-photon system in a microwave cavity, New J. Phys. **21** (2019).
[14] N. R. Bernier, L. D. Tóth, A. K. Feofanov, and T. J. Kippenberg, Level attraction in a microwave optomechanical circuit, Phys. Rev. A **98**, 023841 (2018).
[15] M. Goryachev, W. G. Farr, D. L. Creedon, Y. Fan, M. Kostylev, and M. E. Tobar, High-Cooperativity Cavity QED with Magnons at Microwave Frequencies, Phys. Rev. Appl. **2**, 054002 (2014).
[16] Y. Tabuchi, S. Ishino, T. Ishikawa, R. Yamazaki, K. Usami, and Y. Nakamura, Hybridizing Ferromagnetic Magnons and Microwave Photons in the Quantum Limit, Phys. Rev. Lett. **113**, 083603 (2014).
[17] X. Zhang, C.-L. Zou, L. Jiang, and H. X. Tang, Strongly Coupled Magnons and Cavity Microwave Photons, Phys. Rev. Lett. **113**, 156401 (2014).
[18] H. Huebl, C. W. Zollitsch, J. Lotze, F. Hocke, M. Greifenstein, A. Marx, R. Gross, and S. T. B. Goennenwein, High Cooperativity in Coupled Microwave Resonator Ferrimagnetic Insulator Hybrids, Phys. Rev. Lett. **111**, 127003 (2013).
[19] X. Zhang, N. Zhu, C.-L. Zou, and H. X. Tang, Optomagnonic Whispering Gallery Microresonators, Phys. Rev. Lett. **117**, 123605 (2016).
[20] J. A. Haigh, S. Langenfeld, N. J. Lambert, J. J. Baumberg, A. J. Ramsay, A. Nunnenkamp, and A. J. Ferguson, Magneto-optical coupling in whispering-gallery-mode resonators, Phys. Rev. A **92**, 063845 (2015).
[21] A. Osada, R. Hisatomi, A. Noguchi, Y. Tabuchi, R. Yamazaki, K. Usami, M. Sadgrove, R. Yalla, M. Nomura, and Y. Nakamura, Cavity Optomagnonics with Spin-Orbit Coupled Photons, Phys. Rev. Lett. **116**, 223601 (2016).
[22] V. Baltz, A. Manchon, M. Tsoi, T. Moriyama, T. Ono, and Y. Tserkovnyak, Antiferromagnetic spintronics, Rev. Mod. Phys. **90**, 015005 (2018).
[23] C. Tzschaschel, K. Otani, R. Iida, T. Shimura, H. Ueda, S. Günther, M. Fiebig, and T. Satoh, Ultrafast optical excitation of coherent magnons in antiferromagnetic NiO, Phys. Rev. B **95**, 174407 (2017).
[24] A. Qaiumzadeh, L. A. Kristiansen, and A. Brataas, Controlling chiral domain walls in antiferromagnets using spin-wave helicity, Phys. Rev. B **97**, 020402(R) (2018).
[25] A. N. Bogdanov, U. K. Rößler, M. Wolf, and K.-H. Müller, Magnetic structures and reorientation transitions in noncentrosymmetric uniaxial antiferromagnets, Phys. Rev. B **66**, 214410 (2002).
[26] A. Janutka and P. Gawronski, Structure of magnetic domain wall in cylindrical microwire, IEEE Trans. Magn. **51**, 2374555 (2014).
[27] C. B. Muratov, V. V. Slastikov, A. G. Kolesnikov, and O. A. Tretiakov, Theory of the Dzyaloshinskii domain-wall tilt in ferromagnetic nanostrips, Phys. Rev. B **96**, 134417 (2017).
[28] J. Graf, H. Pfeifer, F. Marquardt, and S. Viola Kusminskiy, Cavity optomagnonics with magnetic textures: Coupling a magnetic vortex to light, Phys. Rev. B **98**, 241406(R) (2018).
[29] H.-B. Braun, J. Kulda, B. Roessli, D. Visser, K. Krämer, H.-U. Güdel, and P. Böni, Emergence of soliton chirality in a quantum antiferromagnet, Nat. Phys. **1**, 159 (2005).
[30] Y. Ichiraku, R. Takeda, S. Shimono, M. Mito, Y. Kubota, K. Inoue, and Y. Kato, Magnetic phase diagram and chiral soliton phase of chiral antiferromagnet $[NH_4][Mn(HCOO)_3]$, J. Phys. Soc. Jpn. **88**, 094710 (2019).
[31] B. A. Ivanov and A. K. Kolezhuk, Solitons with Internal Degrees of Freedom in 1D Heisenberg Antiferromagnets, Phys. Rev. Lett. **74**, 1859 (1995).
[32] I. G. Bostrem, J.-i. Kishine, and A. S. Ovchinnikov, Transport spin current driven by the moving kink crystal in a chiral helimagnet, Phys. Rev. B **77**, 132405 (2008).
[33] J.-i. Kishine, I. G. Bostrem, A. S. Ovchinnikov, and Vl. E. Sinitsyn, Coherent sliding dynamics and spin motive force driven by crossed magnetic fields in a chiral helimagnet, Phys. Rev. B **86**, 214426 (2012).
[34] G. Tatara, H. Kohno, and J. Shibata, Microscopic approach to current-driven domain wall dynamics, Phys. Rep. **468**, 213 (2008).
[35] E. G. Tveten, A. Qaiumzadeh, O. A. Tretiakov, and A. Brataas, Staggered Dynamics in Antiferromagnets by Collective Coordinates, Phys. Rev. Lett. **110**, 127208 (2013).
[36] D. Bouzidi and H. Suhl, Motion of a Bloch Domain Wall, Phys. Rev. Lett. **65**, 2587 (1990).
[37] O. A. Tretiakov, D. Clarke, G.-W. Chern, Ya. B. Bazaliy, and O. Tchernyshyov, Dynamics of Domain Walls in Magnetic Nanostrips, Phys. Rev. Lett. **100**, 127204 (2008).
[38] E. G. Tveten, T. Müller, J. Linder, and A. Brataas, Intrinsic magnetization of antiferromagnetic textures, Phys. Rev. B **93**, 104408 (2016).
[39] E. G. Tveten, A. Qaiumzadeh, and A. Brataas, Antiferromagnetic Domain Wall Motion Induced by Spin Waves, Phys. Rev. Lett. **112**, 147204 (2014).
[40] S. K. Kim, Y. Tserkovnyak, and O. Tchernyshyov, Propulsion of a domain wall in an antiferromagnet by magnons, Phys. Rev. B **90**, 104406 (2014).
[41] D. Bang, P. V. Thach, and H. Awano, Current-induced domain wall motion in antiferromagnetically coupled structures: Fundamentals and applications, J. Sci.: Adv. Mater. Devices **3**, 389 (2018).
[42] D. Lachance-Quirion, Y. Tabuchi, A. Gloppe, K. Usami, and Y. Nakamura, Hybrid quantum systems based on magnonics, Appl. Phys. Express **12**, 070101 (2019).
[43] I. Proskurin, A. S. Ovchinnikov, J.-I. Kishine, and R. L. Stamps, Cavity optomechanics of topological spin textures in magnetic insulators, Phys. Rev. B **98**, 220411(R) (2018).
[44] O. Knudsen, The Faraday effect and physical theory, 1845–1873, Archive History Exact Sci. **15**, 235 (1976).
[45] J. P. van der Ziel, P. S. Pershan, and L. D. Malmstrom, Optically-Induced Magnetization Resulting from the Inverse Faraday Effect, Phys. Rev. Lett. **15**, 190 (1965).
[46] T. Conzelmann, S. Selzer, and U. Nowak, Domain walls in antiferromagnets: The effect of Dzyaloshinskii-

Moriya interactions, J. Appl. Phys. **127**, 223908 (2020).
[47] N. Papanicolaou, Dynamics of domain walls in weak ferromagnets, Phys. Rev. B **55**, 12290 (1997).
[48] N. Papanicolaou, Antiferromagnetic domain walls, Phys. Rev. B **51**, 15062 (1995).
[49] J. Lan, W. Yu, and J. Xiao, Antiferromagnetic domain wall as spin wave polarizer and retarder, Nat. Commun. **8**, 178 (2017).
[50] B. A. Ivanov, Spin dynamics of antiferromagnets under action of femtosecond laser pulses (review article), Low Temp. Phys. **40**, 91 (2014).
[51] J. M. D. Coey, *Magnetism and Magnetic Materials* (Cambridge University Press, Cambridge, UK, 2010).
[52] H.-B. Braun, Fluctuations and instabilities of ferromagnetic domain-wall pairs in an external magnetic field, Phys. Rev. B **50**, 16485 (1994).
[53] J. Vandermeulen, B. Wiele, A. Vansteenkiste, B. Waeyenberge, and L. Dupré, A collective coordinate approach to describe magnetic domain wall dynamics applied to nanowires with high perpendicular anisotropy, J. Phys. D **48**, 035001 (2015).
[54] A. Kirilyuk, A. V. Kimel, and T. Rasing, Ultrafast optical manipulation of magnetic order, Rev. Mod. Phys. **82**, 2731 (2010).
[55] T. S. Parvini, V. A. S. V. Bittencourt, and S. V. Kusminskiy, Antiferromagnetic cavity optomagnonics, Phys. Rev. Res. **2**, 022027(R) (2020).
[56] S. Kusminskiy, *Quantum Magnetism, Spin Waves, and Light* (Springer, New York, 2018).
[57] M. Peck, Y. Huh, R. Skomski, R. Zhang, P. Kharel, M. Allison, D. Sellmyer, and M. Langell, Magnetic properties of NiO and (Ni, Zn)O nanoclusters, J. Appl. Phys. **109** (2011).
[58] H. Kondoh, Antiferromagnetic resonance in NiO in far-infrared region, J. Phys. Soc. Jpn. **15**, 1970 (1960).
[59] D. Stancil and A. Prabhakar, Spin Waves: Theory and Applications (Springer, New York, 2009).
[60] S. Sharma, B. Z. Rameshti, Y. M. Blanter, and G. E. W. Bauer, Optimal mode matching in cavity optomagnonics, Phys. Rev. B **99**, 214423 (2019).